

Microbathymetry inferences from two AUV dives over a short segment of the Central Indian Ridge between 10°18' and 10°57'S, Indian Ocean

**K. A. Kamesh Raju^{1,2*}, V. Yatheesh¹, A. Srinivas Rao^{1,2}, L. Surya Prakash^{1,2}, Durbar Ray¹,
Abhay Mudholkar¹, Kiranmai Samudrala^{1,3}, Nico Augustin⁴, P. John Kurian²**

¹ CSIR-National Institute of Oceanography, Dona Paula, Goa -403004, India

² National Center for Polar and Ocean Research, MoES, Vasco-da-Gama, Goa-403804, India

³ CSIR-National Geophysical Research Institute, Hyderabad – 500007, India

⁴ GEOMAR Helmholtz Centre for Ocean Research, D-24148 Kiel, Germany

*Corresponding author: Kamesh Raju K.A., National Center for Polar and Ocean Research, MoES, Vasco-da-Gama, Goa-403804, India. E-mail: kameshraju@gmail.com

Abstract

Topographic fabric of the rift valley floor has been analyzed using the multibeam echo sounder data obtained by the autonomous underwater vehicle (AUV) Abyss at two locations over a short segment of the slow spreading Central Indian Ridge between 10°18'S and 10°57'S. The region is influenced by hydrothermal venting in the near vicinity. Two AUV dives D51 and D52 were performed over this segment at two locations that are 30 km apart and covered 5 km² and 8 km² seafloor area respectively. The dive D51 covered the off axis part of the rift valley floor in the middle part of the segment, and the dive D52 is located near to the non-transform discontinuity that covered the terminal part of an oceanic core complex (OCC). High resolution seafloor topography as revealed by the AUV mounted multibeam echosounder system brought out several micro bathymetric features such as, a lava lake, a cratered volcano, an OCC, and the foot wall volcanic complex at the distal part of the OCC. The valley floor imaged in the D51 is marked by a lava flow encompassing an area of 1 km² and a volcano in the NE corner. The volcano has a diameter of about 800 m with an elevation of about 200 m from the adjacent seafloor, and the partially mapped volcano crater has a relief of about 60 m. A prominent linear fissure running parallel to the ridge axis has been identified, this feature joins with the volcano. Analysis of AUV mounted CTD data indicated three distinct temperature spikes ranging 0.009 to 0.013°C in the region of dive D51. The observed temperature spikes appear to be related to the linear fissure on the seafloor and probably represent leaky venting of fluids from the fissure. With respect to the dive D52, the foot wall volcanic features associated with the OCC are prominent. The volcanic seafloor feature covered an area of 3.45 km² and is conspicuous with rugged topographic fabric at the base of the OCC. These inferences and the morphotectonics of the rift valley floor as revealed by the AUV data suggest moderate hydrothermal venting in this segment of the slow spreading Central Indian Ridge.

Keywords: Central Indian Ridge, volcano, OCC, turbidity, AUV, CTD

1. Introduction

Autonomous under water vehicles (AUVs) are being increasingly used to map hydrothermal vent fields, including sub-meter nested scale surveys in conjunction with remotely-operated vehicles (ROVs) or human occupied submersibles (Ferrini et al., 2007; Fornari et al. 2004; Kelley et al. 2005; Shank et al. 2011; Yoerger et al. 2007). Typical exploration strategy is to detect the hydrothermal plumes in the water column based on shipborne surveys and then identify and map the active vent fields using AUVs and ROV or human occupied submersible. Introduction of AUVs facilitated the exploration of larger areas more efficiently. Hundreds of small volcanoes have been mapped over the rift valley floor of the Mid Atlantic Ridge (MAR) (Smith and Cann, 1990) using the shipboard multi-beam bathymetry system. Our ability to map the abundance of the volcanic features on the rift valley floor of the Mid Ocean Ridge (MOR) system has increased with the advent and application of AUV based near seabed mapping tools (Jamieson et al. 2014 and Clague et al. 2020). The analysis of high-resolution (1m) bathymetry (microbathymetry), provided an alternative method for identifying hydrothermal deposits by making use of the distinct morphology of sulfide deposits consisting of chimneys and mounds at the Endeavour Segment of the Juan de Fuca (JDF) Ridge (Jamieson et al. 2014 and Clague et al. 2020). Further, the high resolution near seabed data (acoustic, CTD and photography) provided great insights in to the tectonic and magmatic process at the dynamic divergent plate boundaries that are the most potential zones for hosting hydrothermal mineral deposits and home for exotic biological communities (Haase et al. 2007, 2009). Exploration of oceanic core complexes (OCC) over the Mid-Atlantic Ridge (MAR) found that these features host active hydrothermal vents, show extinct hydrothermal deposits, or both (e.g., Logatchev, TAG, Semenov, Lost City, Rainbow, Ashadze, and Von Damm) (Andreani et al. 2014; Dymant et al., 2009; Fruh-Green et al. 2003; German et al. 2010; McCaig et al., 2007; Ondreas et al. 2012; Pertsev et al. 2012; Petersen et al. 2009; Tivey et al. 2003). The recent microbathymetry data over the OCCs enhanced our knowledge about the processes related to detachment faults and their influence on hydrothermal activity (Escartin et al. 2017). The near seabed investigations, in-situ observations and sampling are both technologically challenging and very expensive. This could be one of the reasons for their limited use over the slow spreading ridge segments of the Indian Ocean.

The slow spreading Central Indian Ridge (CIR) has prominent signatures of mantle upwelling and oceanic core complexes (Kamesh Raju et al. 2015; Pak et al. 2017). The Edmond, Kairei, Dodo and Solitaire were the only four vent fields over the CIR, that are confirmed by the visual observations using ROVs and manned submersibles (Gamo et al. 2001; Van Dover et al. 2001; Kawagucci et al.

2008, 2016; Nakamura et al. 2012; Okino et al. 2015). The recent near seabed investigations using deep-tow systems provided visual confirmation of four more active hydrothermal vent fields over the northern part of CIR between 8°-12°S (Kim et al. 2020).. We need to have a better understanding of the OCCs of the central Indian ridge, which are much less investigated. Here we present the microbathymetry and temperature data obtained from the first AUV investigations over the CIR around 10°30'S. The segment surveyed is influenced by hydrothermal venting in the near vicinity as reported by the recent investigations (Son et al. 2014; Kim et al. 2020; Ray et al. 2020). The microbathymetry data are derived from the multibeam echo sounder data obtained by the AUV Abyss at two locations over a short segment of the CIR between 10°18'S and 10°57'S. The observed temperature anomalies and, the presence of a cratered volcano suggest diffuse venting, and the volcanic seafloor identified at the base of the OCC could be a favorable site for the presence of an inactive vent field over this ~70 km long segment of the CIR.

2. Geological setting

CIR is segmented by number of NE-SW trending transform faults and is characterized by slow spreading rate (Engel and Fisher, 1975; DeMets et al. 1990). Full spreading rates varying from 26 to 38 mm/yr were inferred based on magnetic anomaly identifications (Kamesh Raju et al. 2012). The computed spreading rate of the segment in the present study area is 37.3 mm/y (Pak et al. 2017). The recently discovered four vent sites on the CIR by Kim et al. (2020) are located on Segment 1 (north of Vema fracture zone), Segment 2 and Segment 3. The vent field in the Segment 1 (see Figure 1a of Kim et al., 2020) is at the base of an OCC, two sites on the Segment 2 are in a ridge parallel off-axis zone, and the fourth site the “Onnuri Vent Field (OVF)” is located on the summit of an OCC (Kim et al. 2020) on the segment 3 (Fig. 1a). The AUV dives of the present study are located on Segment 3. The multibeam bathymetry map generated using the shipboard data (Fig. 1b) shows that the ridge segment between 10°18'S and 10°57'S is bounded by distinct transform offset in the north and a non-transform discontinuity (NTD) at the southern end (Ray et al., 2020). The ridge segment is characterized by well-defined rift valley with steep walls. The rift valley is wide (18 km) and deep (4500 m) at the northern end and it is relatively shallow (3000 m) and narrow (8 km) at the central part of the segment. The valley floor depth increases to 3600 m towards the NTD in the south (Fig. 1b). The southern end of the valley joins the adjacent ridge segment through an oblique trough (Pak et al. 2017). Slow spreading ridges are characterized by magmatic and amagmatic sections (Kamesh Raju et al. 2008; Pak et al. 2017). The morphotectonic characters suggest that the surveyed segment is in a magmatic phase of evolution (Son et al., 2014 and Pak et al., 2017).

The rift valley floor as seen by the AUV photos is covered by small pillow and eroded basalts, at some places; they are partially enveloped by a layer of sediment (Ray et al. 2020). Petrological analysis of the rocks from the southern end of the valley (between 10°51'S and 10°54'S) exhibited compositions of ultramafic, gabbro, and enriched and transition basalts (Yi et al. 2014). Mantle derived rocks were recovered from an OCC (Pak et al., 2017) at the southern end of the segment 3 (Fig. 1a).

3. Data

The data were acquired during *ORV Sagar Nidhi* cruise SN-48. Physical properties of the water column were obtained by using CTD and the Miniature Autonomous Plume Recorder (MAPR) sensors (NOAA-PMEL USA). More details regarding the water column data collection and results and the shipboard multibeam data were presented in Ray et al. (2020). Here we describe the AUV based data used for the present study. The AUV Abyss of IFM (Institut für Meereskunde) -GEOMAR was used for acquiring the high resolution microbathymetry, CTD (conductivity, temperature and pressure) and turbidity data. High resolution bathymetry data was acquired by using RESON Seabat 7125 multibeam operated at 200 kHz and the AUV is equipped with SBE49 CTD unit to acquire CTD data and a SEAPOINT turbidity sensor. Navigation of the AUV was achieved by bottom transponders that were deployed in the survey area. The AUV was flown at 140 m above the seafloor in bottom tracking mode and a track spacing of 300 m was maintained to achieve 100% insonification of the seafloor. The collected bathymetric data were processed with Reson PDS2000™ software. Grid size of 1m was used to prepare the bathymetry maps (Figs. 2 and 4). The dive D51 was selected based on the shipboard multibeam data to be in the middle of the surveyed ridge segment where the rift valley shallows to about 3000 m. CTD data was processed using standard SBE (Seabird Electronics) software. The potential temperature was computed by using the MATLAB routine (module SW ptmp). Potential temperature variations and turbidity data along selected AUV tracks are presented in Figs. 3 and 5.

4. Results

4.1. AUV dive D51- Microbathymetry of rift valley floor, potential temperature anomalies and cratered volcano

An area of about 5 km² was covered during this dive (Fig. 2). The depths within the dive area varied from 3200 to 3500 m. The dive location is slightly off-axis and encompasses a neo-volcanic ridge that runs parallel to the ridge axis. The deeper portion of the rift valley with smooth seafloor probably represents the exposed lava plain, whereas the shallow portion to the north appears to be sediment covered rocky substratum (Fig. 2), rift seafloor images presented by Ray et al. (2020) suggest sediment

covered valley floor. This covers an area of about 1.2 km² extending sub-parallel to the ridge axis with a maximum width of about 500 m (Fig. 2). The microbathymetry studies carried out over at 45°N MAR show that median valley and the neo volcanic ridges are surrounded by areas of hummocky volcanic terrain or flat sediment covered lava regions (Searle et al., 2010 and Yeo and Searle, 2013). The neo-volcanic ridge with a maximum relief of about 200 meters is defined by elevated mounds ranging in height of 10 to 85 m.

A cratered volcano which is not resolved from the shipboard data is prominently seen on the microbathymetry map prepared from the AUV data (Figs. 2 and 3). The volcano has a relief of 200 m from the adjacent rift valley floor and has a diameter of about 800 m. From the partial coverage of the top of the volcano, it is observed that the crater has a relief of about 60 m (Fig. 2). The top of the volcanic ridge is marked by a fissure like feature (Fig. 2). The fissure feature merges with the base of the cratered volcano towards NNE corner covered by the dive.

We examined the potential temperatures computed from the temperature data recorded by the CTD sensor along all the tracks of the AUV. Distinct temperature spikes/anomalies at three locations are noticed along the tracks that cover the fissure like feature observed on the bathymetry map (Fig. 3a). The characteristics of the observed temperature spikes are listed in Table 1. The observed anomalies though very small in magnitude ranging from 0.009 to 0.013°C are nevertheless distinctive relative to the adjacent potential temperature values along the tracks P1 & P2. The temperature anomalies t1 and t2 are observed on the adjacent tracks and probably belong to the same water mass layer. Another prominent anomaly, t3 was observed on the flank of the volcano (Fig. 3). We also observed some potential temperature spikes and turbidity anomalies on top of the crater, however, we cannot rule out the possibility of noise due to sharp changes in bathymetry. These anomalies need further confirmation.

4.2 AUV dive D52 - Impression of OCC and volcanic seafloor as revealed by the microbathymetry.

The dive D52 covered an area of about 8 km² near to the intersection of an NTD and the ridge axis (Fig. 1). This dive covers a part of the OCC (OCC3-1, Fig.1a) identified in this region based on distinct corrugations observed in the shipboard bathymetry data (Son et al. 2014; Kim et al., 2020). The depth in the dive region varied from 3400 to 3900 m, the deepest portions are observed in the transform region and the shallowest is on the OCC feature (Fig. 4). The microbathymetry map documented distinct undulations on the flanks of the OCC and the steep slope marking the termination of the detachment fault (Fig. 4) that merges on to a corridor of smooth seafloor defining the apron (Escartin et al. 2017). Chaotic topographic fabric revealed by several elevated mounds is seen towards further

west of the apron, this region marks the volcanic seafloor (Figs. 4 and 5a). The termination fault, the apron (Escartin et al. 2017) and the volcanic seafloor defined by the rugged seafloor are conspicuous along the cross profiles (Fig. 5d).

We have examined the potential temperature variations along the tracks P3 and P4 (Fig. 5b and c). Unlike the dive D51, no significant temperature spikes are observed along these tracks. Ray et al. (2020) have reported significant backscatter signature and elevated concentrations of DMn (dissolved manganese concentration in seawater) around 300 m above the seafloor close to this dive (Fig. 1b). The results of Ray et al. (2020) suggest the possibility of high temperature venting in the near vicinity of dive D52. Further, the bulk geochemical composition of ferromanganese encrustations (scraped-off from the rocks) from the flank of the OCC (10°47.62'S; 66° 30.27'E; water depth 2741 m) clearly shows the prominent negative cerium anomaly ($Ce/Ce^*=0.75$ after PAAS normalization) which indicates the contribution from the local hydrothermal activity (Surya Prakash et al., 2020) and substantiates the argument of high temperature venting in the vicinity.

5. Discussion

The dive D51 was over a shallow rift valley floor in the center of the segment. The shallow rift valley floor is supported by relatively thicker crust and can be magmatically active (Lin et al., 1990; Kamesh Raju et al., 1997). The presence of the neo-volcanic ridge and the cratered volcano suggest magmatism with active dikeing. The linear fissure like feature identified on the off-axis rift valley floor observed in the microbathymetry of the dive D51 appears to be the result of a recent magmatic episode and may facilitate hydrothermal activity. We examine the extent of hydrothermal activity based on microbathymetry and the physical signatures in the water column. The heat transfer between the mantle and the hydrosphere at the plate boundaries happens majorly through the magmatism and the hydrothermal activity. Dike intrusion events with or without surface expression of lava flow appear to modulate the hydrothermal activity over the fast spreading ridges (Delaney et al. 1998). In contrast, many hydrothermal vent fields over the slow spreading ridges are controlled by well-developed fluid circulation channeled by the deep fractures connected to magma lenses (e.g. Singh et al. 2006). At slow-spreading ridges periods of volcanic activity may be followed by long episodes of tectonic activity. Slow spreading ridges with high magma budget and thick crust are more favorable zones for dikeing and eruptions than the ridge segments with normal thickness (Sinton et al, 2005). Therefore, it is plausible that hydrothermal systems of short duration are established in the ridge domains with thick crust. It has been documented that the large and long lived (1000s of years) hydrothermal systems like TAG and Snake pit over slow spreading ridges (Lalou et al. 1990) are supported by the fractures

reaching to the magma chamber (Singh et al., 2006). Fast cooling of the dike within a few weeks (Cherkaoui et al. 1997) probably prevents the establishment of long-lived hydrothermal vent systems. However, low temperature, diffuse venting is found at the slow-spreading ridges (German et al. 1994; Botz et al. 1999). Haase et al. (2007) reported hydrothermal venting associated with extremely fresh lava flows at an elevated, apparently magmatically robust segment of the slow-spreading southern Mid-Atlantic Ridge. These studies have suggested that the volcanic eruption events in the near vicinity can influence the hydrothermal activity and induce shallow magmatic activity. Further it is possible that the seamount-dominated axial volcanism will create a crustal structure very different from classic fissure-fed models (Smith and Cann, 1990). It is suggested that the axial volcanism is supported by the shallow magma lenses and support hydrothermal systems that are relatively short lived (~100s of years) (Haase et al., 2009), compared to the long lived systems (1000s of years) that are typically linked to the magma chamber through the deep running fractures (Lalou et al. 1990; Singh et al., 2006). Further, a comparative study of slow spreading ridges such as Mid-Atlantic Ridge and Carlsberg Ridge suggest that the segments with NTD's characteristic of slow and ultra-slow spreading centres, have an axial valley of varying depth with one or more axial volcanic ridges (Murton and Rona, 2015). The observed temperature spikes near to the seafloor at 140 m above the seafloor could be indicators of the diffuse venting taking place in the region. Hydrothermal plume signatures in the water column were reported adjacent to the dive area (Son et al., 2014). These inferences suggest the neo-volcanic ridge could be a possible target to explore for hydrothermal sulphide deposits.

The microbathymetry derived from the dive D52 is dominated by the presence of an OCC and the related morphotectonic features. OCCs have been identified along several segments of Atlantic, Indian, and Arctic Ocean spreading centers. The oceanic detachment faults that are integral part of the OCCs are thought to exhume lower crustal and upper mantle rocks to the seafloor (Blackman et al. 1998; Cannat et al. 2006; Dick, 1989; Karson and Dick, 1983; Tucholke et al. 1998). The OCCs are often characterized by corrugations extending up to tens of kilometers perpendicular to the ridge axis. Evolution of these morphotectonic features lead to the definition of a discrete mode of seafloor spreading (Escartín et al. 2008; Escartín & Canales, 2011; Ohara et al. 2001; Smith et al. 2006).

Recent studies have shown that there is a strong relationship between the OCCs and hydrothermal activity (Escartin et al. 2017). The morphotectonic features identified on the seafloor like the apron suggests a zone of debris shed from the undulated detachment fault surface. The presence of apron is suggested to be the spread of rubble resulting from the continued extension of the underlying detachment fault (Escartin et al. 2017). A similar rubble cover was observed at the incipient 16°36'N

corrugated fault surface on slow spreading MAR (Parnell-Turner et al. 2018). With reference to the present study (Dive D52) we have identified a zone of smooth strip on the microbathymetry map at the base of the undulated fault zone and termed it as the apron zone. In the absence of optical imagery at this location we identified apron zone based on microbathymetry. The presence of this feature may indicate active detachment fault.

In the present study, the volcanic seafloor identified further west of the apron feature (Fig. 5) is associated with the tectono-magmatic activity related to the evolution of the OCC and the detachment fault. Ray et al. (2020) suggested the possibility of high temperature venting in the near vicinity of dive D52. The temperature and turbidity data of dive D52 do not show any anomalies that directly indicate hydrothermal activity. However, active hydrothermal vents could exist in the neighborhood. Several extinct hydrothermal fields near 13°30'N detachment over the MAR were identified by the Russian researchers (Cherkashev et al. 2013; Cherkashov et al. 2017, 2010; Pertsev et al. 2012) using deep-towed self-potential system, TV-camera tows and sampling. These data and results clearly demonstrate that hydrothermal activity has been dominant in space and time throughout the exposed detachment fault surface, from its termination near the ridge axis to the corrugated surface. In addition to inactive hydrothermal fields, an active hydrothermal field (Semenov-2) was also observed (Beltenev et al. 2007; Cherkashov et al. 2010; Pertsev et al. 2012). These studies and the recent investigations on JDF Ridge (Jamieson et al. 2014 and Clague et al. 2020) indicate that the active and inactive hydrothermal fields co-exist or exist in very close proximity. These inferences and the observations in the present study indicate that the distal region of the OCC with the characteristics of volcanic seafloor can be a suitable location for the presence of extinct hydrothermal fields.

6. Conclusions

Microbathymetry obtained from the AUV mounted multibeam bathymetric system has brought out fissure-like feature on the seafloor running parallel to the ridge axis on the rift valley floor this feature is a part of the neo-volcanic ridge. The temperature spikes observed in the dive D51 appear to be emanating from the mapped fissure structure.

A prominent volcano with a cratered top located on the rift valley floor has been imaged in the dive D51. Lava lake and a sedimented seafloor domain that are parallel to the ridge axis have been identified on the rift valley floor.

Dive 52 has imaged the flanks of the OCC and the morphotectonic features such as the corrugated surface of the OCC, an apron zone identified based on smooth topography at the end of the steep slope,

and a domain of volcanic seafloor characterized by rugged topography at the distal end of the OCC are identified. The existence of chemical and physical signatures in the water column suggesting high temperature hydrothermal vent activity in the near vicinity increases the probability of occurrence of inactive hydrothermal mounds in the zone of volcanic seafloor. Further near seabed investigations with ROV and precise sampling is required to confirm this interpretation and to assess the seafloor massive sulfide resource potential of this zone.

Acknowledgements

The authors thank Prof. Sunil Kumar Singh, Director, CSIR-NIO and Dr. M. Ravichandran, Secretary, MoES and former Director NCPOR for encouraging this study. The data was acquired as a part of the Ministry of Earth Sciences, Govt. of India funded program. Thanks to the captain and crew members of *ORV Sagar Nidhi-48* cruise for their support. Authors are thankful to the ABYSS, GEOMAR team and to Dr. Colin Devey, GEOMAR for providing the AUV and the coordinating the AUV charter process. All the figures are plotted with the Generic Mapping Tools (Wessel et al., 2019). Authors thank Dr. Gabriele Uenzelmann-Neben, Editor, Geo-Marine Letters for the encouragement. Authors thank the reviewer Dr. M. Rodriguez and other anonymous reviewers for encouraging comments, critical review and suggestions that helped us to improve the MS. This is CSIR-NIO contribution xxxx and NCPOR contribution xxxx.

References

- Andreani M, Escartin J, Delacour A, et al (2014) Tectonic structure, lithology, and hydrothermal signature of the rainbow massif (Mid-Atlantic Ridge 36° 14'N). *Geochem, Geophys Geosys* 15:3543–3571. <https://doi.org/10.1002/2014GC005269>
- Beltenev V., et al. (2007) A new hydrothermal field at 13°30'N on the Mid-Atlantic Ridge. *InterRidge News* 16, 10–11.
- Blackman DK, Cann JR, Janssen B, Smith DK (1998) Origin of extensional core complexes: Evidence from the Mid-Atlantic Ridge at Atlantis fracture zone. *J Geophys Res Solid Earth* 103:21315–21333. <https://doi.org/10.1029/98jb01756>
- Botz R, Winckler G, Bayer R, et al (1999) Origin of trace gases in submarine hydrothermal vents of the Kolbeinsey Ridge, north Iceland. *Earth Planet Sci Lett* 171:83–93. [https://doi.org/10.1016/S0012-821X\(99\)00128-4](https://doi.org/10.1016/S0012-821X(99)00128-4)
- Cannat M, Sauter D, Mendel V, et al (2006) Modes of seafloor generation at a melt-poor ultraslow-spreading ridge. *Geology* 34:605–608. <https://doi.org/10.1130/G22486.1>
- Cherkaoui ASM, Wilcock WSD, Baker ET (1997) Thermal fluxes associated with the 1993 diking event on the CoAxial segment, Juan de Fuca Ridge: A model for the convective cooling of a dike. *J Geophys Res Solid Earth* 102:24887–24902. <https://doi.org/10.1029/97jb02123>

- Cherkashev GA, Ivanov VN, Bel'tenev VI, et al (2013) Massive sulfide ores of the northern equatorial Mid-Atlantic Ridge. *Oceanology* 53:607–619. <https://doi.org/10.1134/S0001437013050032>
- Cherkashov G, Kuznetsov V, Kuksa K, et al (2017) Sulfide geochronology along the Northern Equatorial Mid-Atlantic Ridge. *Ore Geol Rev* 87:147–154. <https://doi.org/10.1016/j.oregeorev.2016.10.015>
- Cherkashov G, Poroshina I, Stepanova T, et al (2010) Seafloor massive sulfides from the northern equatorial Mid-Atlantic ridge: New discoveries and perspectives. *Mar Georesources Geotechnol* 28:222–239. <https://doi.org/10.1080/1064119X.2010.483308>
- Clague DA, Martin JF, Paduan JB, et al (2020) Hydrothermal Chimney Distribution on the Endeavour Segment, Juan de Fuca Ridge. *Geochem, Geophys, Geosys* 21:. <https://doi.org/10.1029/2020GC008917>
- Connelly DP, Copley JT, Murton BJ, et al (2012) Hydrothermal vent fields and chemosynthetic biota on the world's deepest seafloor spreading centre. *Nat Commun* 3:. <https://doi.org/10.1038/ncomms1636>
- Delaney JR, Kelley DS, Lilley MD, et al (1998) The quantum event of oceanic crustal accretion: Impacts of diking at mid-ocean ridges. *Science* 281:222–230
- DeMets C, Gordon RG, Argus F et al (1990) Current plate motions. *Int J Geophys* 101:425–478
- Dick HJB (1989) Abyssal peridotites, very slow spreading ridges and ocean ridge magmatism. *Geol Soc Spec Publ* 42:71–105. <https://doi.org/10.1144/GSL.SP.1989.042.01.06>
- Dyment, J., Bissessur, D., et al (2009) Detailed investigation of hydrothermal site Rainbow, Mid-Atlantic Ridge, 36°13'N: Cruise MoMARDream. *InterRidge News* 19:22-24.
- Engel CG, Fisher RL (1975) Granitic to ultramafic rock complexes of the Indian Ocean ridge system, western Indian Ocean. *Bull Geol Soc Am* 86:1553–1578. [https://doi.org/10.1130/0016-7606\(1975\)86<1553:GTURCO>2.0.CO;2](https://doi.org/10.1130/0016-7606(1975)86<1553:GTURCO>2.0.CO;2)
- Escartín J, Canales JP (2011) Detachments in Oceanic Lithosphere: Deformation, Magmatism, Fluid Flow, and Ecosystems. *Eos, Trans Am Geophys Union* 92:31–31. <https://doi.org/10.1029/2011eo040003>
- Escartín J, Mével C, Petersen S, et al (2017) Tectonic structure, evolution, and the nature of oceanic core complexes and their detachment fault zones (13°20'N and 13°30'N, Mid Atlantic Ridge). *Geochem, Geophys, Geosys* 18:1451–1482. <https://doi.org/10.1002/2016GC006775>
- Escartín J, Smith DK, Cann J, et al (2008) Central role of detachment faults in accretion of slow-spreading oceanic lithosphere. *Nature* 455:790–794. <https://doi.org/10.1038/nature07333>
- Ferrini VL, Fornari DJ, Shank TM, et al (2007) Submeter bathymetric mapping of volcanic and hydrothermal features on the East Pacific Rise crest at 9°50'N. *Geochem, Geophys, Geosys*: <https://doi.org/10.1029/2006GC001333>

- Fornari DJ, Tivey M, Schouten H, et al (2004) Submarine lava flow emplacement at the east pacific rise 9° 50' N: Implications for uppermost ocean crust stratigraphy and hydrothermal fluid circulation. In: Geophysical Monograph Series. pp 187–217
- Früh-Green GL, Kelley DS, Bernasconi SM, et al (2003) 30,000 Years of hydrothermal activity at the Lost City vent field. *Science* 301:495–498. <https://doi.org/10.1126/science.1085582>
- Gamo T, Chiba H, Yamanaka T, et al (2001) Chemical characteristics of newly discovered black smoker fluids and associated hydrothermal plumes at the Rodriguez Triple Junction, Central Indian Ridge. *Earth Planet Sci Lett* 193:371–379. [https://doi.org/10.1016/S0012-821X\(01\)00511-8](https://doi.org/10.1016/S0012-821X(01)00511-8)
- German CR, Bowen A, Coleman ML, et al (2010) Diverse styles of submarine venting on the ultraslow spreading Mid-Cayman Rise. *Proc Natl Acad Sci U S A* 107:14020–14025. <https://doi.org/10.1073/pnas.1009205107>
- German CR, Briem J, Chin C, et al (1994) Hydrothermal activity on the Reykjanes Ridge: the Steinahóll vent-field at 63°06'N. *Earth Planet Sci Lett* 121:647–654. [https://doi.org/10.1016/0012-821X\(94\)90098-1](https://doi.org/10.1016/0012-821X(94)90098-1)
- Haase KM, Koschinsky A, Petersen S, et al (2009) Diking, young volcanism and diffuse hydrothermal activity on the southern Mid-Atlantic Ridge: The Lilliput field at 9°33'S. *Mar Geol* 266:52–64. <https://doi.org/10.1016/j.margeo.2009.07.012>
- Haase KM, Petersen S, Koschinsky A, et al (2007) Young volcanism and related hydrothermal activity at 5°S on the slow-spreading southern Mid-Atlantic Ridge. *Geochemistry, Geophys Geosystems* 8:. <https://doi.org/10.1029/2006GC001509>
- Jamieson JW, Clague DA, Hannington MD (2014) Hydrothermal sulfide accumulation along the Endeavour Segment, Juan de Fuca Ridge. *Earth Planet Sci Lett* 395:136–148. <https://doi.org/10.1016/j.epsl.2014.03.035>
- Kamesh Raju KA, Ramprasad T, et al (1997), Geophysical investigations over a segment of the Central Indian Ridge, Indian Ocean. *Geo-Marine Letters*,17: 195-201
- Kamesh Raju KA, Chaubey AK, Amarnath D, Mudholkar A (2008) Morphotectonics of the Carlsberg Ridge between 62°20' and 66°20'E, northwest Indian Ocean. *Mar Geol* 252:120–128. <https://doi.org/10.1016/j.margeo.2008.03.016>
- Kamesh Raju KA, Samudrala K, Drolia RK, et al (2012) Segmentation and morphology of the Central Indian Ridge between 3°S and 11°S, Indian Ocean. *Tectonophysics* 554–557:114–126. <https://doi.org/10.1016/j.tecto.2012.06.001>
- Kamesh Raju KA, Abhay V, Samudrala K (2015) Slow Spreading Ridges of the Indian Ocean : An Overview of Marine Geophysical Investigations. *J Indian Geophys Union* 19:137–159
- Karson JA, Dick HJB (1983) Tectonics of ridge-transform intersections at the Kane fracture zone. *Mar Geophys Res* 6:51–98. <https://doi.org/10.1007/BF00300398>

- Kawagucci S, Miyazaki J, Noguchi T, et al (2016) Fluid chemistry in the Solitaire and Dodo hydrothermal fields of the Central Indian Ridge. *Geofluids* 16:988–1005. <https://doi.org/10.1111/gfl.12201>
- Kawagucci S, Okamura K, Kiyota K, et al (2008) Methane, manganese, and helium-3 in newly discovered hydrothermal plumes over the Central Indian Ridge, 18°-20°S. *Geochem, Geophys, Geosys* 9: <https://doi.org/10.1029/2008GC002082>
- Kelley DS, Karson JA, Früh-Green GL, et al (2005) A serpentinite-hosted ecosystem: The Lost City hydrothermal field. *Science* 307:1428–1434. <https://doi.org/10.1126/science.1102556>
- Kim J, Son SK, Kim D, et al (2020) Discovery of Active Hydrothermal Vent Fields Along the Central Indian Ridge, 8–12°S. *Geochemistry, Geophys Geosystems* 21:. <https://doi.org/10.1029/2020GC009058>
- Lalou C, Thompson G, Arnold M, et al (1990) Geochronology of TAG and Snakepit hydrothermal fields, Mid-Atlantic Ridge: Witness to a long and complex hydrothermal history. *Earth and Planetary Science Letters* 97:113-128. [https://doi.org/10.1016/0012-821X\(90\)90103-5](https://doi.org/10.1016/0012-821X(90)90103-5).
- Lalou C (1993) New age data for Mid-Atlantic Ridge hydrothermal sites: TAG and Snakepit chronology revisited. *J Geophys Res* 98:9705–9713. <https://doi.org/10.1029/92JB01898>
- Lin J, Purdy GM, Schouten H, et al (1990) Evidence from gravity data for focused magmatic accretion along the Mid-Atlantic Ridge. *Nature* 344:627–632. <https://doi.org/10.1038/344627a0>
- Nakamura K, Watanabe H, Miyazaki J, et al (2012) Discovery of new hydrothermal activity and chemosynthetic fauna on the Central Indian ridge at 18°-20°S. *PLoS One* 7:. <https://doi.org/10.1371/journal.pone.0032965>
- Ohara Y, Yoshida T, Kato Y, Kasuga S (2001) Giant Megamullion in the Parece Vela Backarc Basin. *Mar Geophys Res* 22:47–61. <https://doi.org/10.1023/A:1004818225642>
- Okino K, Nakamura K, Sato H (2015) Tectonic background of four hydrothermal fields along the central Indian ridge. In: *Subseafloor Biosphere Linked to Hydrothermal Systems: TAIGA Concept*. pp 133–146
- Ondréas H, Cannat M, Fouquet Y, Normand A (2012) Geological context and vents morphology of the ultramafic-hosted Ashadze hydrothermal areas (Mid-Atlantic Ridge 13N). *Geochem, Geophys, Geosys* 13: <https://doi.org/10.1029/2012GC004433>
- Pak SJ, Moon JW, Kim J, et al (2017) Widespread tectonic extension at the Central Indian Ridge between 8°S and 18°S. *Gondwana Res* 45:163–179. <https://doi.org/10.1016/j.gr.2016.12.015>
- Parnell-Turner RE, Mittelstaedt E, Kurz MD, et al (2018) The Final Stages of Slip and Volcanism on an Oceanic Detachment Fault at 13°48'N, Mid-Atlantic Ridge. *Geochem, Geophys, Geosys* 19:3115–3127. <https://doi.org/10.1029/2018GC007536>
- Pertsev AN, Bortnikov NS, Vlasov EA, et al (2012), Recent massive sulfide deposits of the Semenov ore district, Mid-Atlantic Ridge, 13°31' N: Associated rocks of the oceanic core complex and their hydrothermal alteration. *Geol. Ore Deposits*, 54, 334–346.

- Petersen S, Kuhn K, Kuhn T, et al (2009) The geological setting of the ultramafic-hosted Logatchev hydrothermal field (14°45'N, Mid-Atlantic Ridge) and its influence on massive sulfide formation. *Lithos* 112:40–56. <https://doi.org/10.1016/j.lithos.2009.02.008>
- Ray D, KameshRaju KA, Srinivas Rao A, et al (2020) Elevated turbidity and dissolved manganese in deep water column near 10°47'S Central Indian Ridge: studies on hydrothermal activities. *Geo-Marine Lett* 40:619–628. <https://doi.org/10.1007/s00367-020-00657-5>
- Searle RC, Murton BJ, Achenbach K, et al (2010) Structure and development of an axial volcanic ridge: Mid-Atlantic Ridge, 45°N. *Earth and Planetary Science Letters* 299:228–241. <https://doi.org/10.1016/j.epsl.2010.09.003>.
- Shank T, Fornari D, Yoerger D, et al (2003) Deep submergence synergy: Alvin and ABE explore the Galápagos rift at 86°W. *Eos (Washington DC)* 84:.. <https://doi.org/10.1029/2003EO410001>
- Shank T, James H, Santiago H et al (2011). Discovery of Nascent Vents and Recent Colonization Associated with (Re)activated Hydrothermal Vent Fields by the GALREX 2011 Expedition on the Galápagos Rift. AGU Fall Meeting.
- Singh SC, Crawford WC, Carton H, et al (2006) Discovery of a magma chamber and faults beneath a Mid-Atlantic Ridge hydrothermal field. *Nature* 442:1029–1032. <https://doi.org/10.1038/nature05105>
- Sinton J, Grönvold K, Sæmundsson K (2005) Postglacial eruptive history of the Western Volcanic Zone, Iceland. *Geochem, Geophys, Geosys* 6: <https://doi.org/10.1029/2005GC001021>
- Smith DK, Cann JR (1990) Hundreds of small volcanoes on the median valley floor of the Mid-Atlantic Ridge at 24–30°N. *Nature* 348:152–155. <https://doi.org/10.1038/348152a0>
- Smith DK, Cann JR, Escartín J (2006) Widespread active detachment faulting and core complex formation near 13°N on the Mid-Atlantic Ridge. *Nature* 442:440–443. <https://doi.org/10.1038/nature04950>
- Son J, Pak SJ, Kim J, et al (2014) Tectonic and magmatic control of hydrothermal activity along the slow-spreading Central Indian Ridge, 8S–17S. *Geochemistry, Geophys Geosystems* 15:2011–2020. <https://doi.org/10.1002/2013GC005206>
- Surya Prakash L, Ray D, B. NN, et al (2020) Anomalous phase association of REE in ferromanganese crusts from Indian mid-oceanic ridges: Evidence for large scale dispersion of hydrothermal iron. *Chem Geol* 549:.. <https://doi.org/10.1016/j.chemgeo.2020.119679>
- Tivey MA, Schouten H, Kleinrock MC (2003) A near-bottom magnetic survey of the Mid-Atlantic Ridge axis at 26°N: Implications for the tectonic evolution of the TAG segment. *J Geophys Res Solid Earth* 108:.. <https://doi.org/10.1029/2002jb001967>
- Tucholke BE, Lin J, Kleinrock MC (1998) Megamullions and mullion structure defining oceanic metamorphic core complexes on the Mid-Atlantic Ridge. *J Geophys Res Solid Earth* 103:9857–9866. <https://doi.org/10.1029/98jb00167>
- Van Dover CL, Humphris SE, Fornari D, et al (2001) Biogeography and ecological setting of Indian Ocean hydrothermal vents. *Science* 294:818–823. <https://doi.org/10.1126/science.1064574>

- Wessel, P., Luis, J.F., Uieda, L., et al (2019) The Generic Mapping Tools Version 6. *Geochem, Geophys, Geosys* 20:5556-5564.
- Yeo IA, and Searle RC (2013), High-resolution ROV mapping of a slow-spreading ridge: Mid-AtlanticRidge45N, *Geochem. Geophys. Geosyst* 14:1693–1702. doi:10.1002/ggge.20082.
- Yi SB, Oh CW, Pak SJ, et al (2014) Geochemistry and petrogenesis of mafic-ultramafic rocks from the Central Indian Ridge, latitude 8°-17° S: Denudation of mantle harzburgites and gabbroic rocks and compositional variation of basalts. *Int Geol Rev* 56:1691–1719. <https://doi.org/10.1080/00206814.2014.955539>
- Yoerger DR, Bradley AM, Jakuba M, et al (2007) Mid-ocean ridge exploration with an autonomous underwater vehicle. *Oceanography* 20:52–61. <https://doi.org/10.5670/oceanog.2007.05>

Figure captions:

Figure 1 a) Study area (rectangle box) along with locations of dives indicated by black square areas within the box, projected on the multibeam and tectonic elements map of Kim et al., (2020). Satellite derived gravity map was used as background. Ridge axis is marked by white line, red lines represent transform fault and the white dashed line indicate fracture zones. Star symbols denote the active the vent locations identified by Kim et al., (2020). NTD 3-1 is the non-transform discontinuity between segment 3 and segment 3a OVF is Onnuri Vent Field. b) Shipboard multibeam map of the study area, data from SN-48 cruise. D51 and D52 denote the Abyss AUV dive locations. Red dot is the probable vent location inferred by Ray et al., (2020), yellow dots are the plume locations of Son et al., (2014).

Figure 2 Bathymetry map of dive D51, generated from the AUV mounted multibeam data, the data is gridded at 1m. Contours are at 50 m. Lava plain and sediment covered areas are demarcated. The ridge parallel linear fissure like feature is marked by red dashed line. The partially mapped volcano is prominent in the NNE corner of the map.

Figure 3 a) High resolution bathymetry map derived from AUV mounted multibeam data. AUV track lines where temperature spikes were observed are shown along with the locations of the observed temperature spikes (t1, t2 and t3) indicated by open circle with cross. b) Temperature, turbidity and bathymetry profiles along the track P1. The black dashed line indicates the AUV path with respect to the seafloor. c) Temperature, turbidity and bathymetry profiles along the track P2. Black arrows on profiles P1 and P2 point to the observed temperature spikes. The AUV was flown in bottom tracking mode at an elevation of 140 m above the seafloor. The black dashed line indicates the AUV path with respect to the seafloor.

Figure 4 Bathymetry map of dive D52, generated from the AUV mounted multibeam data, the data is gridded at 1m. Contour interval is 50 m. The outline of the volcanic seafloor complex at the base of the OCC is marked with yellow line.

Figure 5 a) a) High resolution bathymetry map derived from dive D52 AUV mounted multibeam data along with AUV track lines P3 and P4. This dive is devoid of temperature spikes. b) and c) show the temperature, turbidity, and bathymetry along the tracks P3 and P4 respectively, the dashed line indicates the AUV path with respect to the seafloor. d) Profile plots along the near E-W trending lines C1, C2, and C3 are shown along with the morphotectonic elements associated with the OCC. Extent of the identified apron zone is marked by pink color on the profile.

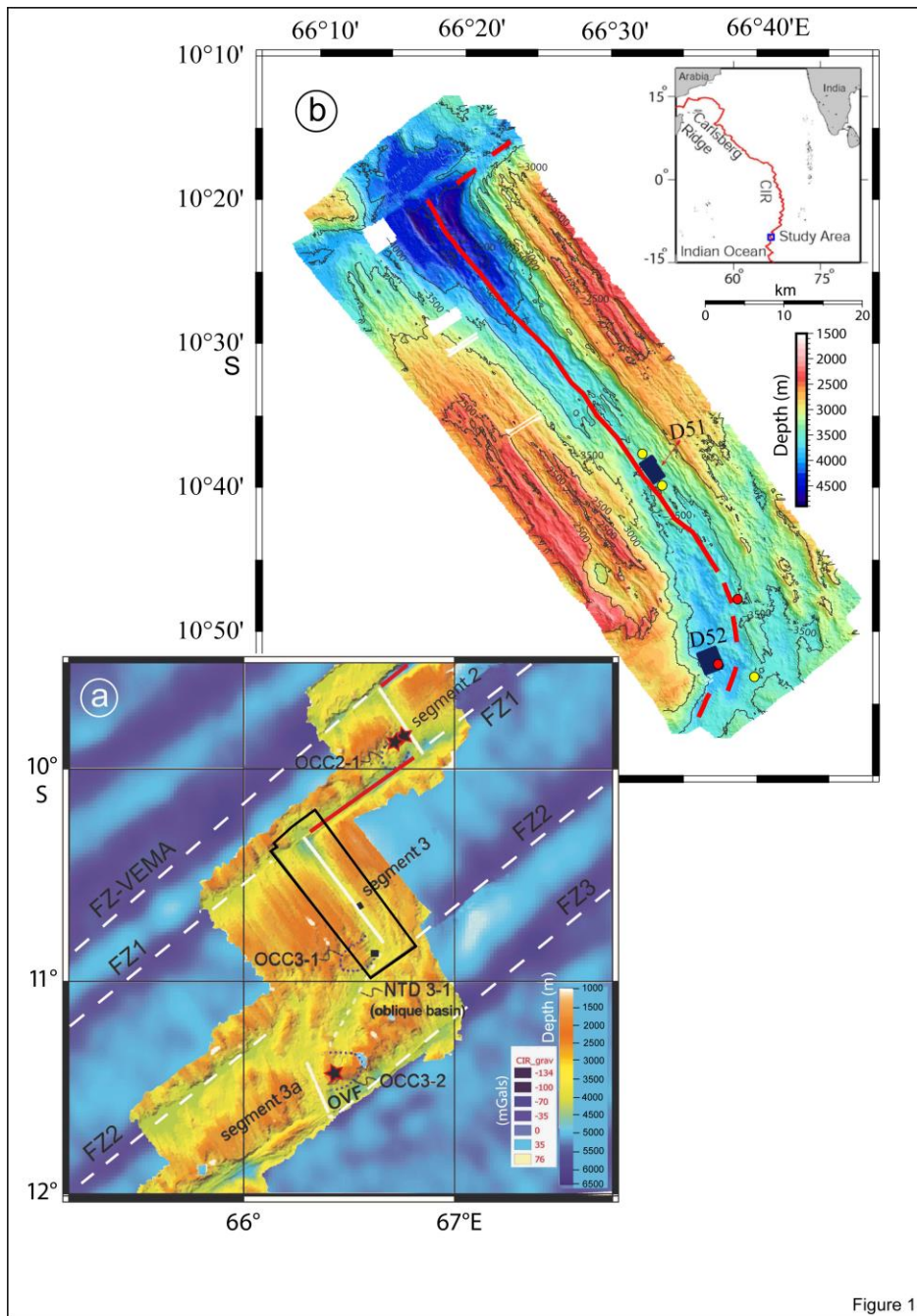


Figure 1

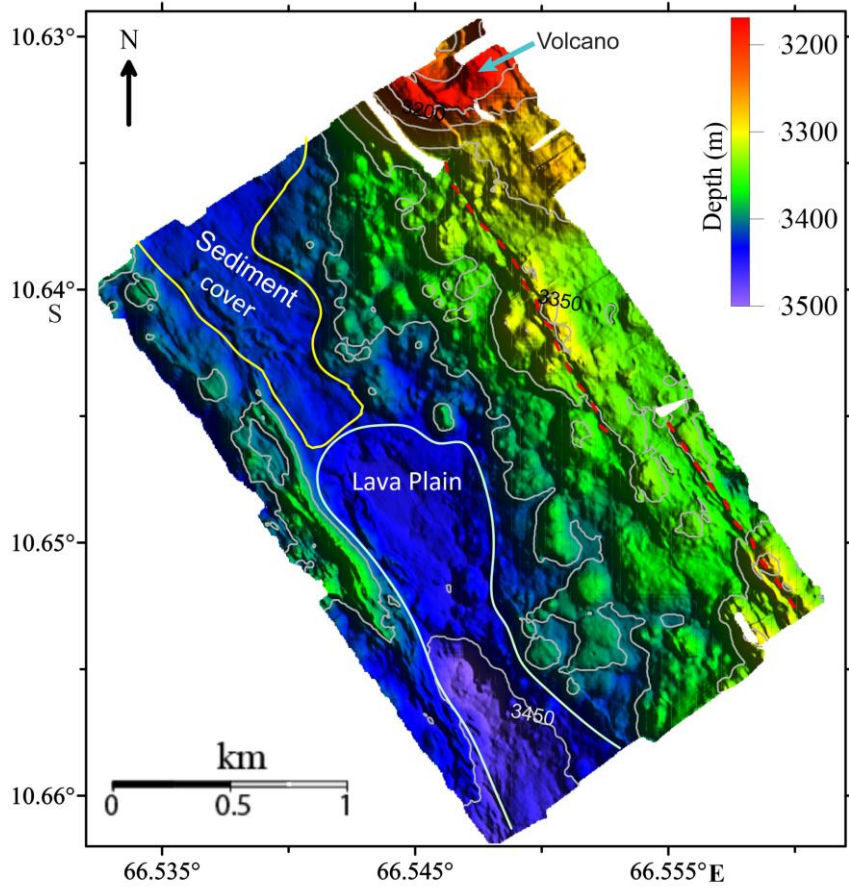


Figure. 2

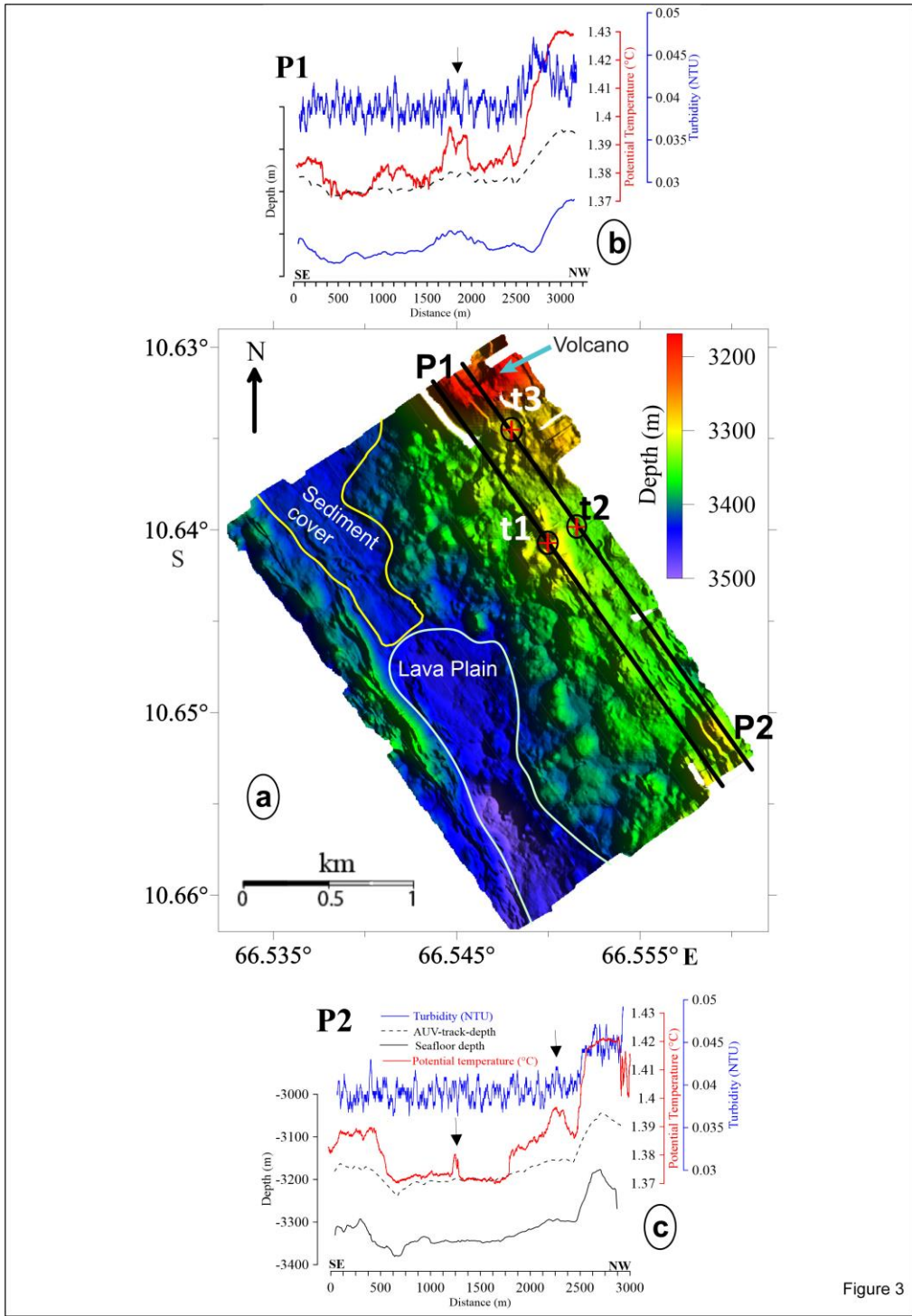


Figure 3

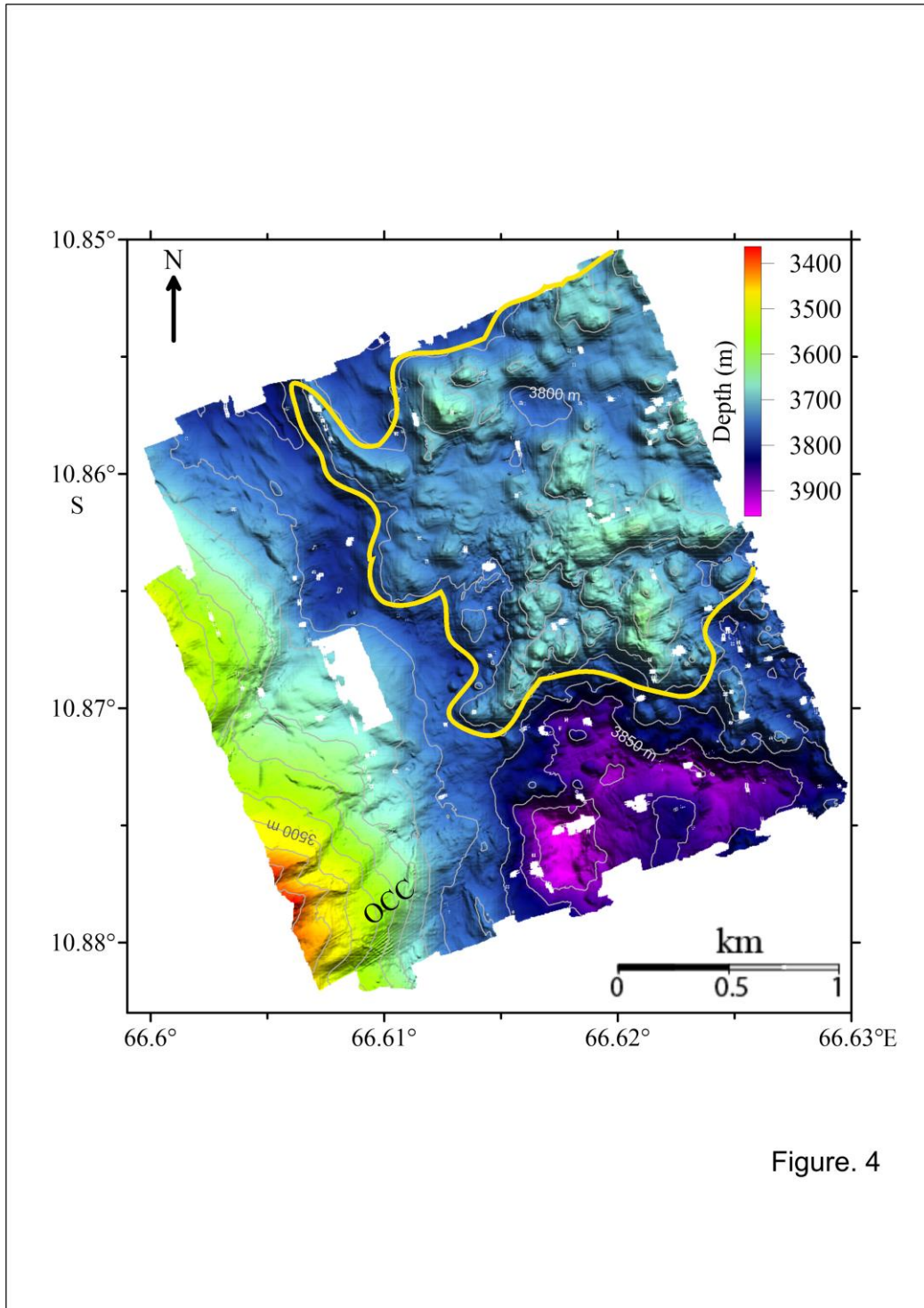


Figure. 4

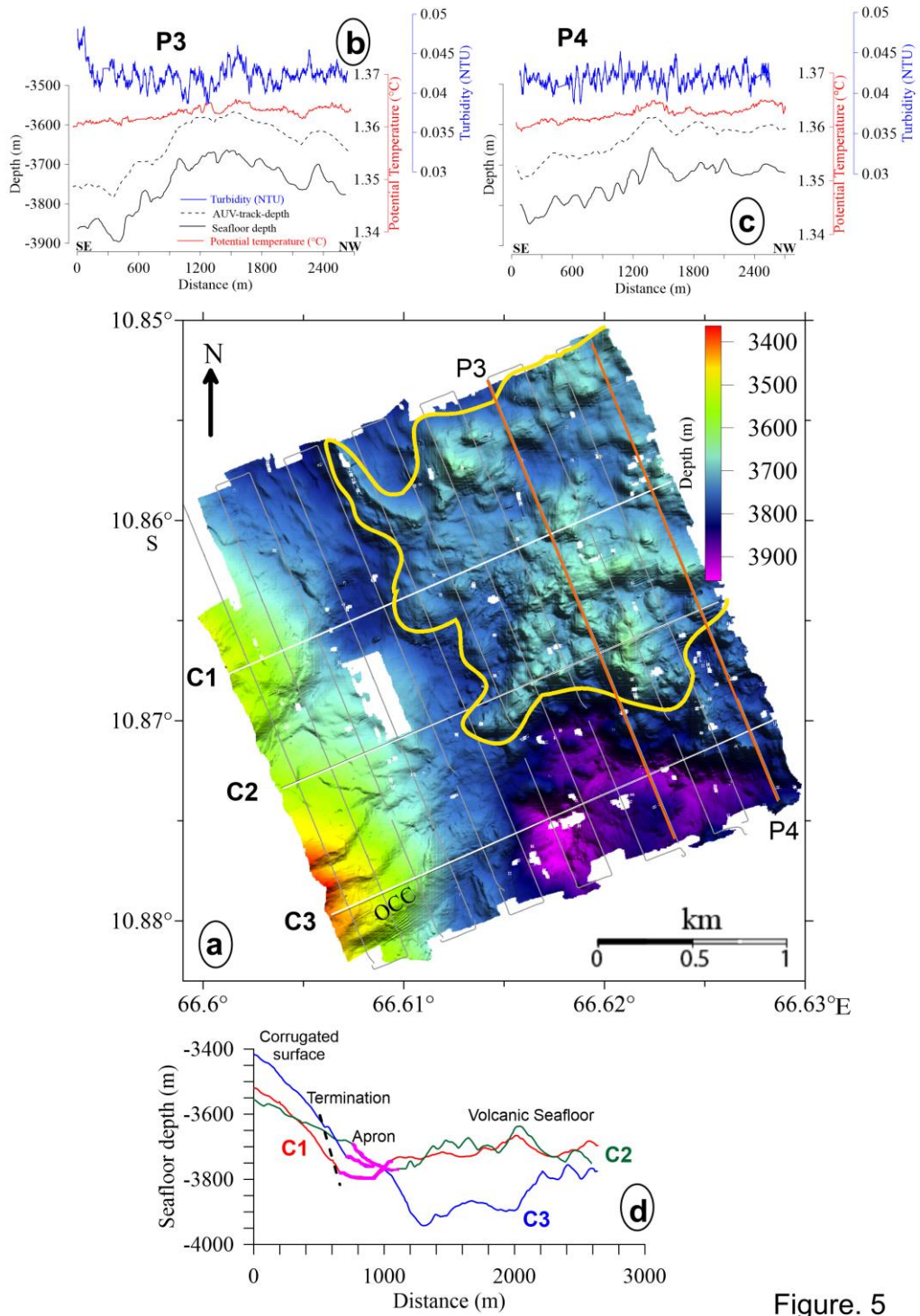


Figure. 5

Table-1 Details of observed temperature anomalies.

S.no	Latitude in degree.	Longitude in degree	Potential temperature Anomaly °C	Depth m	Remarks
t1	10.643	66.555	~0.01	3304	Over the fissure
t2	10.637	66.5497	~0.01	3341	West of fissure
t3	10.641	66.5506	~0.01	3297	On the flank of volcano